Polymer Vol. 39 No. 24 pp. 5939–5948, 1998
0032-3861/98/$ – see front matter

PII: S0032-3861(98)00092-5

Fusion bonding of maleic anhydride grafted polypropylene–polyamide 6 blends to polyamide 6

Jacques-Eric Bidaux[a], Gregory D. Smith[a], Jan-Anders E. Månson[a,*], Christopher J.G. Plummer[b] and Jöns Hilborn[b]
[a]*Laboratoire de Technologie des Composites et Polymères, Ecole Polytechnique Fédérale de Lausanne, CH-1015 Lausanne, Switzerland*
[b]*Laboratoire des Polymères, Ecole Polytechnique Fédérale de Lausanne, CH-1015 Lausanne, Switzerland*
(Received 24 October 1997; accepted 18 December 1997)

Bond formation between maleic anhydride grafted polypropylene–polyamide 6 (PP_g–PA) blends and polyamide 6 (PA) has been investigated. The fracture energy, G_c, of joints formed at various bonding temperatures was measured using a wedge test in a double cantilever beam geometry and compared with that obtained between homopolymers of the constituents. Optical and transmission electron rnicroscopy was used to study the morphology of the blends in the bulk and at the interface, in an effort to understand how the microstructure influences the fracture behaviour. For bonding temperatures, T_b, below the melting temperature of PA, the fracture energy G_c of the bonds between PP_g–PA adherends and the PA adherends is low. G_c nevertheless increases with increasing T_b, reaching a maximum for $T_b \cong 225$°C, which approximately coincides with the melting temperature of PA, and then falling off at higher T_b. Observations of the fracture surfaces using electron spectroscopy for chemical analysis (ESCA) show that fracture occurs cohesively in the blend within a thin layer close to the interface. In the case of blends in which the PP_g is the continuous phase, the presence of the PA domains alters the crack propagation path, leading to an increase in G_c, with increasing PA content. In the case of blends where the PA is the continuous phase, the fracture behaviour depends strongly on bonding temperature. For $T_b < 225$°C, PA is still solid, which prevents intimate contact and interdiffusion across the interface. G_c, is low, and decreases with increasing PA content. For $T_b \geq 225$°C, melting of PA allows interdiffusion of PA chains to occur across the interface, leading to a strong bond. The experimental observations suggest that the crack propagates by jumping between PP_g domains. In this temperature range, G_c is high, and increases with increasing PA content. © 1998 Elsevier Science Ltd. All rights reserved.

(Keywords: fusion bonding; blends; semi-crystalline polymers)

INTRODUCTION

There is a widespread interest in developing materials systems and structures combining existing polymers as in the form of blends, multilayers or coatings. It is well established that interfacial properties play an important role in controlling the overall properties of such multicomponent systems. The mechanisms of interface formation depend strongly on the nature of the polymers to be joined[1]. When two surfaces of the same amorphous homopolymers are brought into intimate contact above T_g, interdiffusion of the polymer chains occurs across the interface. For chains exceeding a critical molecular weight, entanglements will form on both sides of the interface, resulting in a strong bond[2,3]. However, in the case of partially molten semi-crystalline polymers, the presence of the crystalline domains restricts the motion of the molecular chains and severely limits interdiffusion[4]. The bonding temperature must, therefore, be increased to above the melting temperature, T_m, to obtain significant adhesion[5].

In the case of interfaces between dissimilar materials, the situation is even less favourable. Most polymers are incompatible even in the molten state and there is limited interdiffusion[1]. In order to achieve good bonding, a compatibilizer is generally added. A simple example of a compatibilizer is a di-block co-polymer in which the blocks are compatible with, and segregate to opposing sides at the interface. The mechanisms by which block co-polymers, either placed at the interface as an interlayer[6–8] or created *in situ* by chemical reaction[9–14], act at interfaces between amorphous polymers have been studied in detail. The fracture energy of incompatible amorphous interfaces has been successfully modelled in terms of parameters such as the molecular weight and the density of co-polymer per unit area of the interface[15–18]. A strong bond requires the presence of a minimum density of entangled co-polymers straddling the interface, such that this latter can sustain an applied stress higher than the crazing stress of at least one of the two bulk polymers on either side of the interface[7,19].

No doubt, because of its relative complexity, bonding between incompatible and semicrystalline polymers is less well understood at present[19]. Some recent studies suggest that, in such materials, the processing and the microstructure plays a key role in the interfacial fracture energy[20–22]. In the case of maleic anhydride grafted polypropylene–polyamide 6 interfaces, the bond strength has been observed to be strongly affected by melting and further crystallization of

*To whom correspondence should be addressed. Tel: +41-21-693 42 81; Fax: +41-21-693 58 80

both the polypropylene and polyamide 6[20]. A clear step-like increase in fracture energy occurs at bonding temperatures close to the polyamide melting temperature. This abrupt increase in adhesion was explained by the increased mobility of the polyamide chains in the melt and by the co-crystallization of the co-polymer blocks with the crystalline domains on either side of the interface on subsequent cooling. It was shown that in all cases where the adhesion was significant, failure occurred cohesively within polypropylene, but close to the interface, probably owing to the presence of the relatively low molecular weight grafted chains. The important influence of the microstructure on adhesion has also been pointed out by Boucher et al. in a similar system[21,22]. Although for low bonding temperatures, the adhesion could be explained solely in terms of co-polymer areal density and molecular weight, as in the case of amorphous polymers, this picture no longer appeared to be valid for bonding temperatures very close to the polyamide melting temperature. A large unexpected increase in adhesion was observed which seemed to be correlated with the presence of the β crystalline phase on the polypropylene side of the interface. It was concluded that the presence of molecular connecting chains between the polymers is not the only parameter controlling adhesion in semi-crystalline materials. The microstructure of the polymer close to the interface, which controls the size and nature of the deformation zone and the dissipated energy at the crack tip, are equally important.

The present work is focused on the study of the strength of an interface formed between two semi-crystalline materials, in the special case where one of the two adherends is a blend. By using blends of different compositions, various microstructures can be created in the vicinity of the interface. The presence of a second phase is expected to alter the crack propagation path and the deformation mode at the crack tip, modifying the interfacial strength. It has often been observed that the crack propagation path slightly deviates from the interface because of the existence of a weak interfacial region[20,23]. If the crack deviates towards the blend, it is clear that the microstructure of the blend will play a critical role on the fracture energy. The aim of the present work is, therefore, to study the role of the blend microstructure on the strength of the interface. The final goal is to optimize the microstructure of the adherends in order to obtain the maximum interfacial strength.

A series of bonds between maleic anhydride grafted polypropylene–polyamide 6 (PP_g–PA) blends and polyamide 6 (PA) were manufactured. The interfacial fracture energy, G_c of the resulting interfaces was measured for bonding temperatures varying from the melting temperature of PP_g to above that of the PA6. The interfacial fracture energy was then compared with that obtained between homopolymers of the blend constituents. Optical and transmission electron microscopy (TEM) was used to investigate the morphology of the blends in the bulk and at the interface, in an effort to understand its effect on the interfacial fracture energy. Electron spectroscopy for chemical analysis (ESCA) was used to determine the exact locus of failure, that is whether fracture took place at the interface (adhesive failure) or in the bulk of one of the adherends (cohesive failure). Additional measurements by differential scanning calorimetry (DSC) were performed to investigate melting–crystallization behaviour of the respective polymers.

EXPERIMENTAL

The basic materials used in this study were polypropylene homopolymer (PP) grade APPRYL 3050MN1 with M_n = 57 280 and M_w = 275 100, polyamide-6 (PA) grade ORGAMIDE RESNO with M_n = 18 650 and M_w = 37 300, and finally polypropylene grafted with 0.46% maleic anhydride (PP–MAH) grade PPg3050MN1gAM with M_n = 27 900 and M_w = 71 090, all from Elf-Atochern S.A. The grafted polypropylene (PP–MAH) had an average of 1.3 anhydride groups per chain. A blend of the PP homopolymer. and the grafted PP was prepared by mixing PP–MAH resin with pure PP to make a polypropylene blend containing 0.085% MAH (PP_g). This PP_g was mixed with various amnounts of PA to make the 75 wt%PP_g–25 wt%PA, 50 wt%PP_g–50 wt%PA and 25 wt%PP_g–75 wt%PA blends. The blends of the PP, PP–MAH and PA were prepared as follows: The pellets were dried in a vacuum oven at 80°C for 72 h. The required amount of each material was weighed and the pellets mixed and fed into a 16 mm diameter twin screw extruder. The extrudate was pelletized and mixed again. The barrel temperature in the extruder was 180°C for the PP_g blend and 230°C for the PA–PP_g blends. The screw speed was 50 rpm.

Plaques for the bonding experiments were injection moulded. The PA granules were dried in a vacuum at 150°C for 18 h before injection. The size of the plaques was approximately 50 × 50 mm^2, with a thickness ranging from 1.3 to 3 mm, to have a control on the degree of mode mixity[15]. The melt injection temperature was 195°C and 280°C for the PP_g and PA, respectively. The mould temperature was 100°C for both materials. The pressure cycle was also the same for both materials, namely 60 MPa for the injection phase and 30 MPa for the holding phase. In order to avoid contamination, no release agent was used. Plaques containing PA were stored in a sealed container containing a desiccant.

The bonding experiments were conducted using an instrumented matched-die mould installed on a servo-hydraulic load frame. A schematic of the mould with the heating and cooling systems is shown in *Figure 1*. The temperature was monitored by thermocouples located in the upper and lower moulds. Both moulds halves were heated to

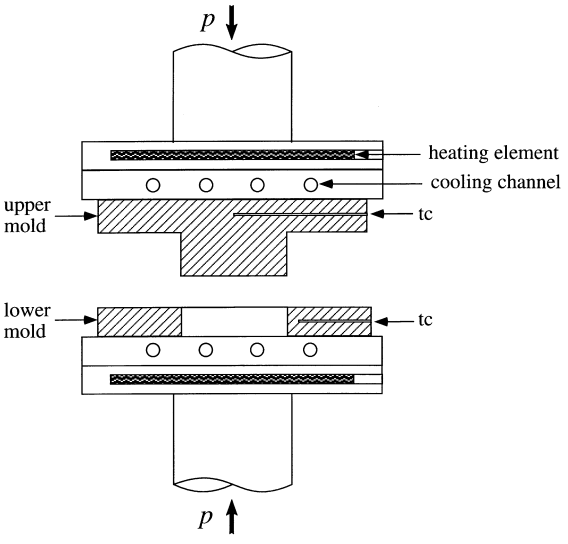

Figure 1 Schematic of the 50 × 50 mm matched-die mould showing the heating elements, cooling channels and thermocouples (tc)

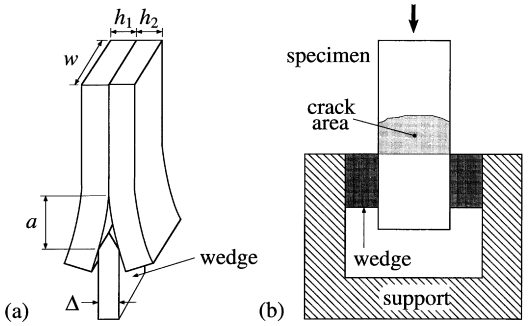

Figure 2 The double cantilever beam geometry with a constant crack opening displacement (wedge test): (a) side view; and (b) front view

the same temperature (±1°C) and allowed to equilibrate at temperature for approximately 10 min. A 5 mm wide strip of 30 μm thick polyimide (KAPTON) tape, was placed on the lower surface adjacent to the polyamide plaque to serve as a crack initiator. Bonds were made by placing both plaques into the mould which was then closed at a pressure of 4 MPa for a hold time of 10 min, at which point the heating was turned off. The initial cooling rate was approximately 55°C min^{-1}. The pressure was maintained until the mould reached room temperature.

The fracture energies of the bonds were measured using a double cantilever beam geometry with a constant crack opening displacement as shown in *Figure 2*. A starter crack was initiated in the fracture specimens by aligning a single edged razor blade with the plane of the interface and pressing it into the specimen. Crack propagation was accomplished by forcing the specimens over the razor blade using a screw driven load frame at a crosshead speed of 2 mm min^{-1}. The crack area was illuminated by placing a lamp behind the specimen and the crack area recorded as a function of sample position using a video camera. The crack length, *a*, was measured at 2.5 mm intervals over a 10 mm length at the mid-point of the specimen (*Figure 2*). The overall crack length at each position was calculated as the average of five crack lengths: one at each edge and the other three evenly spaced across the specimen width. The crack propagation was predominantly stable, but did vary somewhat with position. Occasionally the crack front would reach an area of poor bonding and jump 1 to 2 mm, arresting in an adjacent region of higher toughness, before recommencing stable growth. Only data corresponding to stable growth are reported here.

The critical strain energy release rate, G_c was calculated using an equation derived by Kanninen based on the bending of a prismatic beam supported by an elastic foundation[24]. The key assumptions for this equation are that: (1) the only contribution to the stored elastic energy of the system is from the bending of the free portions of the beams and the elastic deformation ahead of the crack tip; (2) the elastic energy stored ahead of the crack tip is well described by an elastic foundation; and (3) all the elastic energy released upon fracture is absorbed by plastic deformation at the crack tip[6]. For this case G_c is given by

$$G_c = \frac{3\Delta^2 E_1 h_1^3 E_2 h_2^3}{8a^4}\left(\frac{E_1 h_1^3 C_2^2 + E_2 h_2^3 C_1^2}{(E_1 h_1^3 C_2^3 + E_2 h_2^3 C_1^3)}\right) \qquad (1)$$

with $C_1 = 1 + 0.64\, h_1/a$, $C_2 = 1 + 0.64\, h_2/a$, where Δ is the wedge thickness, *E* is the elastic modulus, *h* is the beam thickness, *a* is the crack length and the subscripts 1 and 2 refer to PA and PP_g–PA blends, respectively. Equation (1) is only valid if the crack propagation occurs along the bimaterial interface. According to Xiao *et al.*, for a symmetric double cantilever beam geometry using materials with different elastic moduli, there is a mode II component in the stress intensity factor near the crack tip which causes the crack to grow into the more compliant material (in our case the PP_g–PA blend)[15]. To avoid this, an asymmetric geometry using h_2/h_1, ratios of 2.3 for the PP_g–PA, 75PP_g–25PA/PA, and 50PP_g–50PA/PA bonds, 1.5 for the 25PP_g–75PA/PA bonds, and 1 for the PA/PA bonds were used to force the crack to follow the interface. Equation (1) was also used for calculating the mode I G_c values of bulk and bonded PP_g specimens.

Computation of the fracture energy from equation (1) requires knowledge of the elastic moduli E_1 and E_2 of each material. Since the elastic moduli are time and frequency dependent, it is important to determine the time scale Δ*t* during which stress is applied to a volume element during crack propagation. As a first approximation, Δ*t* can be taken as the time during which a volume element, initially at the crack tip, remains located between the crack tip and the wedge and thus undergoes bending[20]:

$$\Delta t = a/\dot{a} \qquad (2)$$

where *a* is the crack length, $\dot{a}$ is the crack propagation velocity. Accordingly, G_c was computed using the elastic moduli measured dynamically at a frequency *v* given by

$$v = 1/\Delta t = \dot{a}/a \qquad (3)$$

For the crack velocities used in our experiments, this frequency is of the order of 0.01 Hz. The elastic moduli of the samples were measured at room temperature in 3-point bending using a rheometer (Rheometrics RSAII) at 0.016 Hz. The elastic moduli were 1.03 GPa for the pure PP_g resin, 1.10 GPa for the 75PP_g–25PA blend, 1.73 GPa for the 50PP_g–50PA blend, 2.01 GPa for the 25PP_g–75PA blend, and 3.63 GPa for the pure PA resin.

The morphology of the blends and blend–PA interfaces was studied by transmission electron microscopy. Staining was carried out by immersion in 0.2 g $RuCl_3$ $3H_2O$ dissolved in 10 ml of 5.25% aqueous sodium hypochlorite for 24 h. Finally, 100–200 nm thick sections were obtained by microtoming at room temperature using a Reichert–Jung Ultracut-E and examined using a Philips EM430ST transmission electron microscope at 300 kV.

The cross-sectional morphology of the interface was also characterized on a more macroscopic scale using optical microscopy. Microtomed sections, approximately 10 μm thick, were cut perpendicular to the plane of the interface from the edge of the remaining side pieces directly adjacent to the fracture specimen. The central portion of these sections were then viewed between crossed polarizers.

The elemental composition of the bulk samples and the fracture surfaces of the pure resin and the blend adherends were analysed by electron spectroscopy for chemical analysis (ESCA) to determine the path of the crack propagation during fracture. The instrument used was a Perkin–Elmer PHI 5500 spectrometer equipped with an hemispheric detector and an Mg anode. For the experimental conditions used here, the spot size was estimated to be about 0.5 ± 0.1 mm. The fracture surfaces were examined by cutting samples approximately 10 mm by 10 mm, from a remaining piece of the bonded plaque and splitting them open with a razor blade. The sample was then immediately placed in the vacuum chamber of the ESCA apparatus.

The melting and crystallization of the resins were characterized by differential scanning calorimetry (DSC7 form Perkin–Elmer). Samples, 5 ± 0.5 mg, were obtained by punching 3 mm diameter pellets form the as-moulded plaques.

RESULTS

Blend morphology

The morphology of stained thin sections of the blends is shown in *Figure 3*. The staining procedure is much more effective for the PP_g than for the PA and the PP_g appears dark in comparison with the PA. The amorphous regions between the lamellae of the PP, stain more than the crystalline regions, also allowing the lamellae structure to be observed. The morphology of the $75PP_g$–25PA and the $50PP_g$–50PA blends is shown in *Figure 3a* and *b*, respectively. In both cases the blend consists of a continuous matrix of PP_g and dispersed domains of PA. The area fraction of the PA domains in *Figure 3b* is approximately twice that of *Figure 3a*. The domain size is approximately 0.5 μm and is the same for both blends. For the $25PP_g$–75PA blend the continuous phase is PA rather than PP_g. The PP_g domains are approximately the same size as the PA domains in the PP_g-rich blends.

Blends thermal characterization

The melting and crystallization of the pure resins and the blends are compared in *Figure 4*. The onset and peak melting temperatures T_m^{onset} and T_m^{peak}, the heat of melting, ΔH_m, the onset and peak crystallization temperatures, T_c^{onset} and T_c^{peak}, and the heat of crystallization, ΔH_c, of the pure resins and the blends are summarized in *Table 1*. For the pure resins a single peak was observed for melting and crystallization. The behaviour of the blends was more complex with two peaks typically being observed, centred around the melting and crystallization temperatures of the pure resins. The onset melting temperature of the PP_g peak in the blends is within 1°C of that of the pure resin. Moreover, the onset crystallization temperature of the PP_g

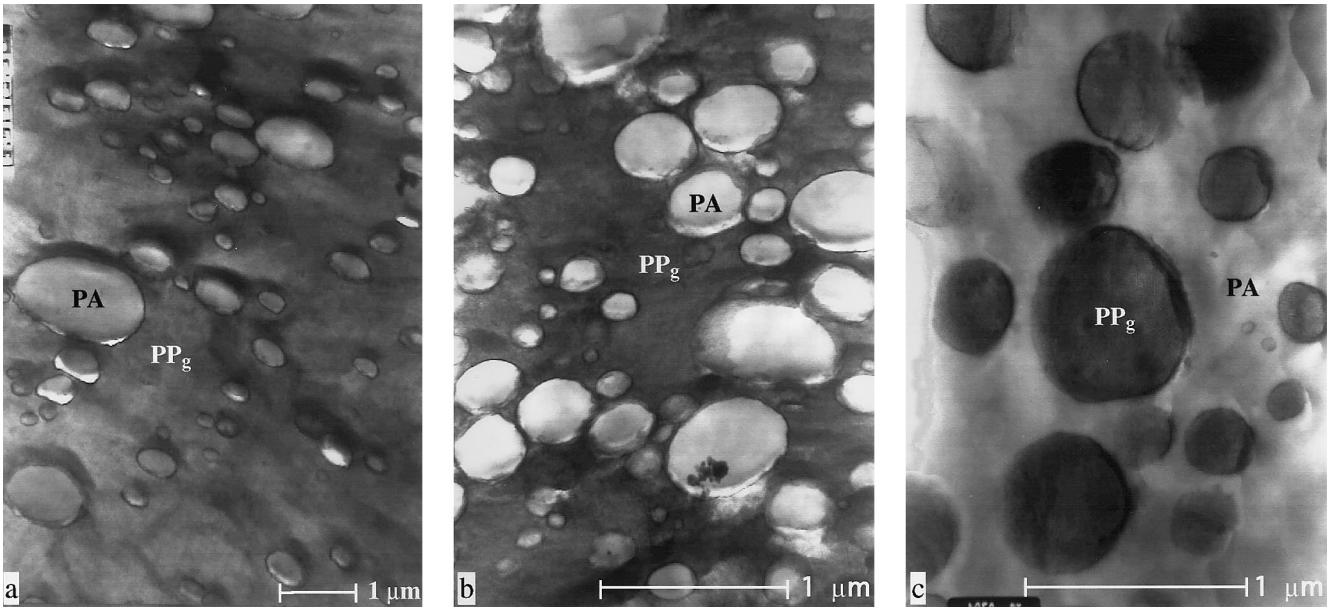

Figure 3 TEM micrographs of blend morphology for: (a) $75PP_g$–25PA; (b) $50PP_g$–50PA; and (c) $25PP_g$–75PA

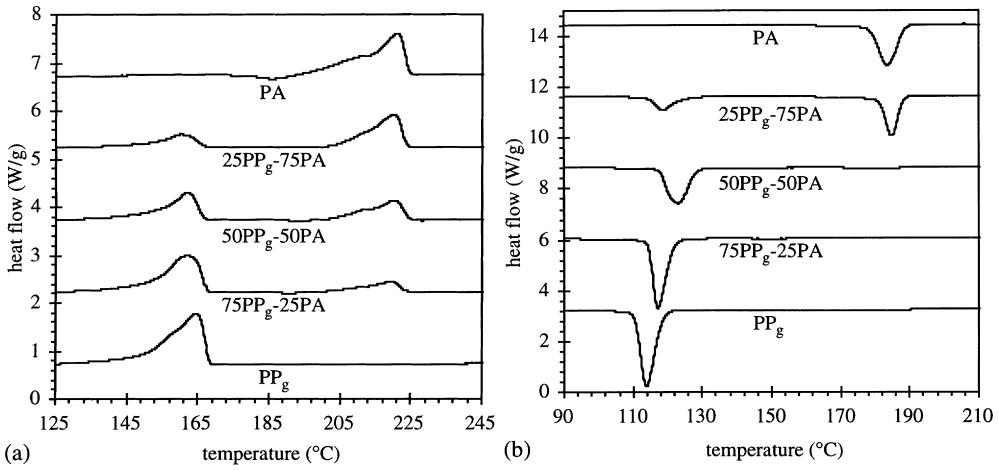

Figure 4 Heat flow as a function of temperature for the pure and blended resins by DSC at 10°C min^{-1}. (a) heating of as-moulded samples; and (b) subsequent cooling

Table 1 Thermal characterization of pure and blended resins by DSC at 10°C min^{-1}. Sample mass was 5 ± 0.5 mg. Units: T_i^{onset}, T_i^{peak} in °C and ΔH_c, in J g^{-1}

Resin	PP_g			PA			PP_g			PA		
	T_m^{onset}	T_m^{peak}	ΔH_m	T_m^{onset}	T_m^{peak}	ΔH_m	T_c^{onset}	T_c^{peak}	ΔH_c	T_c^{onset}	T_c^{peak}	ΔH_c
PP_g	151.5	164.3	75.2				118.0	113.6	92.5			
$75PP_g$–25PA	152.2	−161.8	60.6	199.2	218.8	15.6	121.5	116.8	77.6	—	—	—
$50PP_g$–50PA	153.7	161.8	41.7	202.6	220.0	27.9	127.9	123.0	61.4	187.6	~183.3	3.0
$25PP_g$–75PA	151.0	160.2	21.8	202.9	220.0	40.5	124.1	118.3	24.7	187.8	184.7	41.6
PA				195.3	220.7	59.0				188.3	183.5	63.3

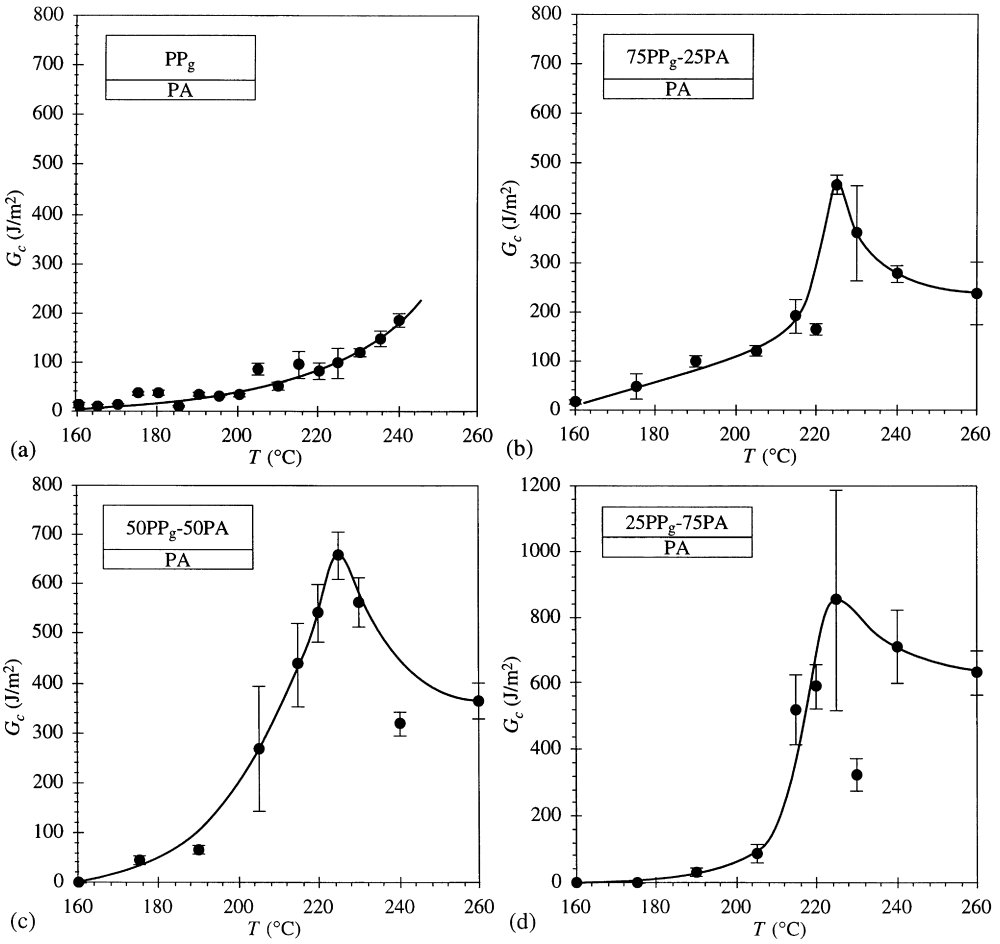

Figure 5 Fracture energy, G_c, as a function of bonding temperature for: (a) PP_g/PA; (b) $75PP_g$–25PA/PA; (c) $50PP_g$–50PA/PA; and (d) $25PP_g$–75PA/PA bonds

peak is between 2–3°C lower for the blends than for the pure PP_g, and decreases with increasing PA content. The onset melting temperature of the PA peak is increased by 4–7°C, and also increases with the PA concentration, whereas T_m^{peak} is unaffected. The ratio of the heat of melting in the blend to that of the pure polymer is approximately equal to the mass fraction of each polymer in the blend. The existence of two separate melting peaks with values of T_m^{onset}, T_m^{peak} and ΔH_m. approximately equal to that of the pure resins shows that the melting of each resin in the blend is unaffected by the presence of the other resin. This was not the case for the crystallization peaks.

The crystallization peaks of the pure PP_g and PA resins were at a distinct and well separated temperature, T_c^{peak} was equal to 118.0°C for the PP_g resin and 183.5°C for the PA. Two crystallization peaks, at roughly the same temperature as in the pure resins, were observed for the $25PP_g$–75PA and $50PP_g$–50PA blends (in this last case the PA peak is hardly visible) but only a single peak, slightly above the crystallization temperature of pure PP_g, was observed for the $75PP_g$–25PA blend. However, the heat of crystallization of the PP_g peak for the blends was larger than one would expect if the ΔH_c, measured for this peak was only due to crystallization of the PP_g. This shows that, in agreement with the results of Moon *et al*., the presence of the PP_g retards crystal nucleation in the PA and PA crystallizes concurrently with the PP_g[25]. According to Moon *et al*., this is due to the small size of the PA domains. For submicron size domains, the probability of finding an heterogeneity which can act as a nuclei for crystallization is very small. This prevents crystallization to occur at the usual temperature. Once PP_g begins to crystallize, heterogeneous sites for the PA become available and PA crystallizes concurrently with the PA.

One can calculate the total heat expected during the crystallization by multiplying the ΔH_c, of each pure resins

by the mass fraction of that resin in the blend. This calculation produces values of 85, 78 and 70 J g^{-1} for the $75PP_g$–25PA, $50PP_g$–50PA, and $25PP_g$–75PA blends, respectively. Summing the measured ΔH_c values of the PP_g and PA peaks for each blend produces values of 77.6, 64.4 and 66.3 J g^{-1} for the $75PP_g$–25PA, $50PP_g$–50PA, and $25PP_g$–75PA blends, respectively. In each case the calculated values are higher than the measured values.

The degree of crystallinity of PA in the blend is, therefore, assumed to be lower than in the pure resin, to an extent which depends on the PA content in the blend. Comparing the measured and calculated values for total heat of crystallization for these blends, the measured value is approximately 10% lower than calculated, for the $75PP_g$–25PA blend, and 20% lower than calculated for the $50PP_g$–50PA blend. The PA is the continuous phase in the $25PP_g$–75PA blend, and therefore the crystallization of the PA is not retarded. The measured heats of crystallization are 6% lower than the calculated values for the $25PP_g$–75PA blend.

Interfacial fracture energies

Plaques of pure PP_g and the blends were isothermally bonded to pure PA plaques, and fracture specimens cut from the bonded plaques. The fracture energy of the bonds between pure PP_g and pure PA adherends is shown in *Figure 5a*. The G_c values increase monotonically with bond temperature. No bonding experiments were performed at bond temperatures below T_m of the polypropylene since previous experiments showed that only very weak bonding was possible below T_m[20]. In contrast to these latter results where there was a sharp increase in G_c values at the melting point of the PA, no such increase is seen here, the G_c values increasing steadily with bonding temperature. The present values of adhesion are also relatively low, with maximum values just below 200 J m^{-2} compared with maximum values of approximately 850 J m^{-2} observed in the previous work where the PP_g resin contained ethylene–propylene rubber (EPR), which increases the toughness of PP[20]. The PP_g resin contains the same amount of MAH as previously, but no EPR, explaining the lower values of G_c.

The G_c values as a function of bonding temperature are shown in *Figure 5b–d* for the $75PP_g$–25PA/PA, $50PP_g$–50PA/PA, and $25PP_g$–75PA/PA bonds, respectively. The general trends in the three figures are similar. The fracture energy increases at an increasing rate as the bonding temperature is increased, and reaches a maximum at 225°C. At higher bonding temperatures the fracture energy decreases. Low fracture energies are observed at temperatures just above the melting temperature of the PP_g (160°C).

To determine the cohesive strength of PA, three additional bonding experiments were carried out. PA/PA bonds were made at temperatures of 210, 225 and 260°C. If the decrease in G_c was due to degradation in PA, a similar decrease should have been observed in the PA/PA bonds. The G_c values for the bond made at 210°C was 53 ± 1 J m^{-2}, approximately half of the value obtained for the $75PP_g$–25PA/PA bond made at 205°C. Two bonds were made at 225°C; the G_c values were 1100 ± 200 J m^{-2} and 1290 ± 190 J m^{-2}. A bond was also made at 260°C, but the adhesion was sufficiently good that the crack could not be made to propagate along the interface, indicating that its G_c was at least equal to that of the bonds made at 225°C. This seems to indicate that the decrease in fracture energy above 225°C is not due to thermal degradation of PA.

Table 2 Elemental compositions of reference surfaces as measured by ESCA and the volume fraction of PA in the blends. Concentrations in atomic percent

Resin	C	O	N	V_{PA}
PP_g	99	1	0	0
$75PP_g$–25PA	97	2	1	0.21
$50PP_g$–50PA	97	2	1	0.44
$25PP_g$–75PA	93	3	4	0.70
PA	78	11	11	1

Composition of fracture surfaces

The results of the ESCA analysis of the reference surfaces for the pure resins and the blends are given in *Table 2*. The elemental compositions represent average compositions taken over the area of the electron beam (about 0.5 mm in diameter). The elemental composition of the PP_g is mostly carbon with a trace of oxygen from the MAH graft. The elemental composition of the PA has the expected ratio of oxygen and nitrogen, with the carbon concentration being slightly higher than the expected value of 75%. The carbon composition of the blend references is higher than one would expect if the area fraction of PA on the cut surface was proportional to the volume fraction of the PA, V_{PA}, in the bulk of the blends. The discrepancy may be due to the way the reference surfaces were prepared. The reference surfaces were made by cutting into the centre of an as-moulded plaque with a razor blade. As the blade passes through the material, it will preferentially cut through the less tough PP_g matrix. Since the PP_g resin is the continuous phase for the $75PP_g$–25PA and $50PP_g$–50PA blends, it is relatively easy for the crack to propagate in the PP_g and avoid the PA domains. However, this is not possible for the $25PP_g$–75PA blend since the continuous phase is the PA, and crack will grow through the PA as it jumps from domain to domain of PP_g.

The ESCA analysis for the fracture surfaces of the bonds made between the pure resins and the blends are given in *Table 3*. The compositions of the PP_g and PA fracture surfaces for the PP_g–PA bond are approximately the same, indicating that the crack preferentially grows through the PP_g. Adjacent fracture surfaces of each of the bonds in *Table 3* have the same compositions. The compositions of

Table 3 Elemental compositions of fracture surfaces of the bonds as measured by ESCA. Concentrations in atomic percent

Bond	T_{bond}	PP_g or blend			PA		
	(°C)	C	O	N	C	O	N
PP_g/PA	225	99	1	0	98	2	0
$75PP_g$-25PA/PA	225	98	1	1	99	1	0
$50PP_g$-50PA/PA	225	99	0	0	99	1	0
$25PP_g$-75PA/PA	225	93	5	2	92	5	3

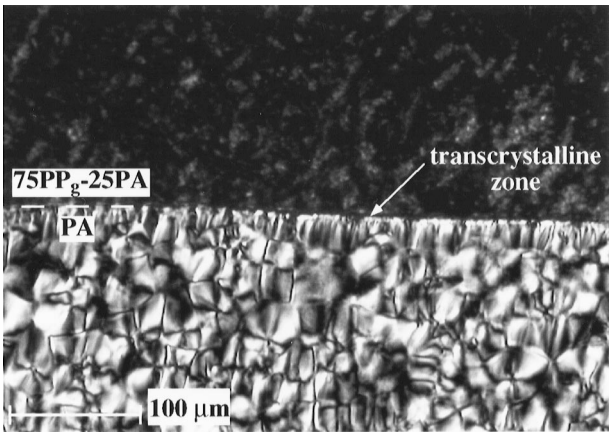

Figure 6 Polarized light micrographs of $75PP_g$–25PA/PA bond interface made at $T_{bond} = 225°C$

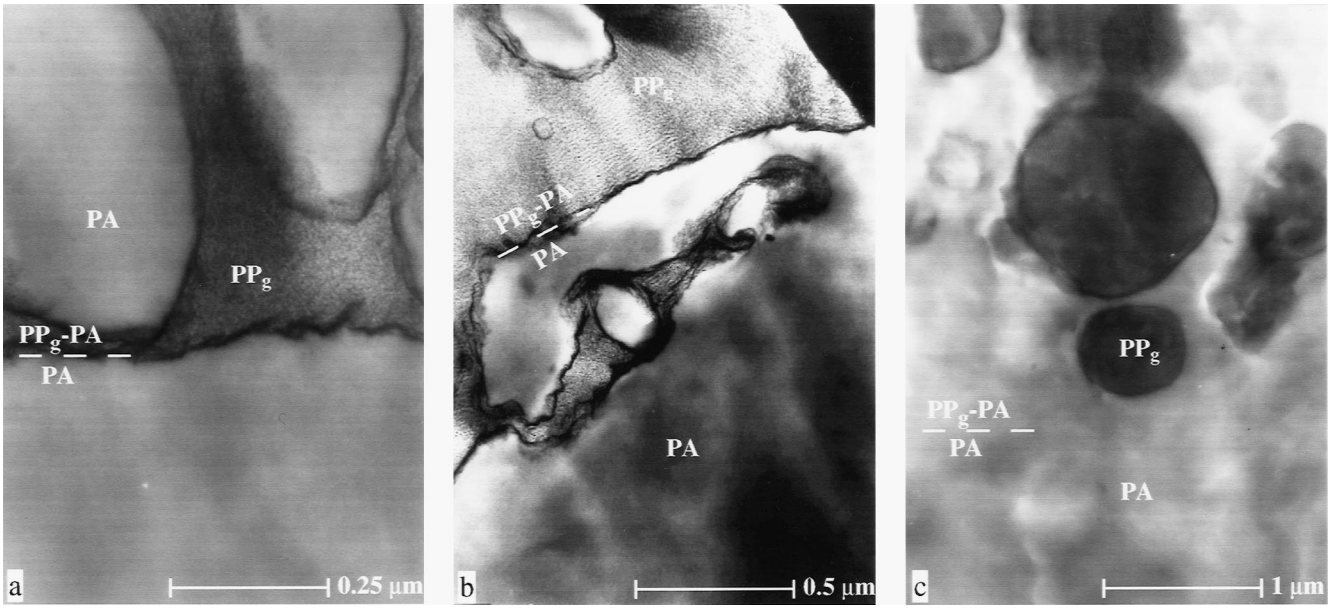

Figure 7 TEM micrographs of the interface of: (a) $75PP_g$–25PA/PA; (b) $50PP_g$–50PA/PA; and (c) $25PP_g$–75PA/PA bonds made at $T_{bond} = 225°C$

the fracture surfaces and the blend reference compositions, *Table 2*, are essentially the same, suggesting that failure was cohesive in the blend adherend.

Bond interface morphology

The cross-sectional morphology of the interface as seen under optical microscopy is shown in *Figure 6* for a $75PP_g$–25PA/PA bond. This morphology is typical for all the bonds made above T_m of the PA. The plane of the interface is essentially flat although some small undulations are occasionally visible over large sections of the interface. The spherulitic structure of the PA is easily distinguished, but not that of the blend. Also visible is a narrow transcrystalline layer in the PA adjacent to the blend interface.

TEM images of interface of the blend–PA bonds for $T_b = 225°C$, i.e. slightly above the melting temperature of PA, are shown in *Figure 7*. The interface of the $75PP_g$–25PA/PA bond, *Figure 7a*, is straight with PA domains very close to the interface but not straddling it. The situation for the interface of the $50PP_g$–50PA/PA bond, *Figure 7b*, is similar, but the interface is rougher, suggesting an increase in interfacial area between the PA and blend adherend. The interface of the $25PP_g$–75PA/PA bond, *Figure 7c*, is different from the previous two bonds in *Figure 7*. In this case the continuous phase in the blend is PA and the interface between the PA and blend adherend has completely healed.

DISCUSSION

Fracture energies

Only relatively low bond strengths, below 200 J m^{-2}, are obtained between pure PP_g and PA adherends (*Figure 5*). A significant difference between these bonds and those between the blend and PA adherends is that no decrease in fracture energy is observed for bonding temperatures above the melting temperature of the PA. The fracture energies of the bonds between the blends and PA in *Figure 5* are more easily compared by plotting the fracture energies at temperatures below the melting temperature, at the melting temperature, and above the melting temperature, as a function of the volume fraction of PA in each blend, as shown in *Figure 8*.

The fracture energies of the bonds made at 205°C are low,

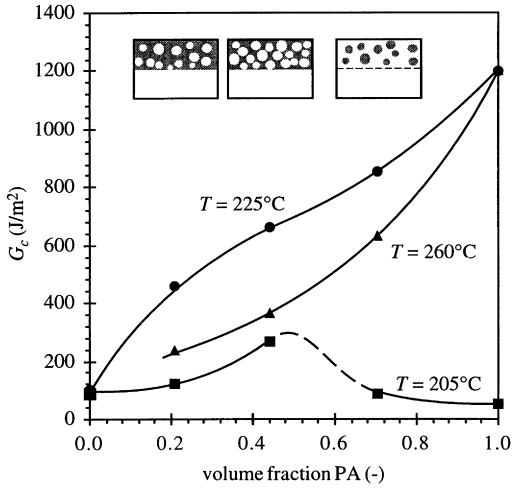

Figure 8 Comparison of the G_c values for temperatures below T_m at T_m, and above T_m as a function of volume fraction PA in the blend

less than 300 J m^{-2} (*Figure 8*). At this bonding temperature, the PP_g resin is well above its melting temperature and the grafted polypropylene chains can move easily to the interface, driven by the reduction in interfacial free energy[20]. Once at the interface, the MAH end-groups can react with amine end-groups at the interface to form a link across the interface. The fracture energies of the bonds where PP_g is the continuous phase increase with increasing PA content. As shown in *Figure 7a*, the interface of 75PP_g–25PA/PA bond is microscopically straight, and the small increase in fracture energy for this bond compared with the PP_g–PA interface is thought to be due to the reinforcing effect of the PA domains. The presence of the PA domains is expected to alter the crack propagation path, leading to higher fracture energies. Since there are about twice as many PA domains in the PA 50PP_g–50PA blend as the 75PP_g–25PA blend, the reinforcement effect of the domains will be larger for the 50PP_g–50PA/PA bond. The result is a fracture energy of 270 J m^{-2} for this bond, more than twice the fracture energy of the 75PP_g–25PA/PA bond. However, if the PA content of the blend is increased to 75%, phase inversion occurs and the continuous phase is PA with inclusions of PP_g. Therefore, in this composition region, G_c decreases when the PA content increases. Since the bonding temperature is 20°C below the melting temperature of PA, low fracture energies are not surprising. Very low fracture energies were observed for PP/PP bonds when the bonding temperature was below the melting temperature of PP[5].

The highest fracture energy of the bonds made at 225°C is for the PA/PA bond, 1300 J m^{-2} whereas the lowest fracture energy bond is for the PP_g/PA bond, 100 J m^{-2} (*Figure 8*). The fracture energies of the blend/PA bonds increase almost linearly with PA content in the blend. The bonding temperature is now just above the melting temperature of PA. Significant interdiffusion is possible between the PA phases contained in the blends and the pure PA. The higher the PA content, the larger the resulting adhesion, in agreement with the maximum fracture energy is found for the PA/PA bond.

The fracture energies of the bonds made at 260°C are, with the exception of the PA/PA bond, less than the fracture energies measured at 225°C. At present, the reason for this decrease in fracture energy is not clear and we shall only mention briefly some of the possible explanations. First of all, the decrease in G_c could be due to thermal degradation. The accumulation at the interface of degradation products and oxidized low molecular weight grafted chains may have created a weak boundary layer at the interface, i.e. a layer with insufficient cohesion to withstand the deformation induced by the fracture test[23]. Although such a weak boundary layer may already exists at relatively low temperature, at high temperature, the mobility of degraded products increases and the problem becomes more pronounced. The decrease in fracture energy could it also be due to a change in the organization of co-polymers at the interface. Such a change was observed by Brown and coworkers who studied the effect of a PS-PMMA co-polymer layer between PS and PMMA adherends[17]. The degree of organization of the co-polymers at the interface, as measured by secondary ion mass spectroscopy (SIMS), was observed to increase when the bonding temperature or bonding time increased, while, at the same time, G_c was observed to decrease. The authors reached the surprising conclusion that a disorganized di-block layer provided a tougher bond than a perfectly organized layer. A maximum in fracture energy versus bonding temperature was observed by Lee *et al.* for polyamide–polystyrene interfaces obtained by reactive compatibilization using a styrene-maleic anhydride (SMA) random co-polymer interlayer[11]. The existence of this maximum was explained by a competition between the rate of diffusion processes and the rate of chemical reaction at the interface. The maximum in fracture energy would correspond to the temperature at which the rate of the two competing mechanisms are comparable. However, it has been shown in detail by Lee *et al.* that, for such a mechanism to work, the interlayer of compatibilizer must be rather thin. In our case, the thickness of the grafted PP sample is large and this interpretation does not seem to apply. Another possibility would be a change of the bulk mechanical properties close to the interface. As pointed out by Creton, interfacial fracture energy is influenced, in the case of high adhesion where a plastic zone forms ahead of the propagating crack tip, by the mechanical properties of a layer with a thickness comparable with the plastic zone width, i.e. several microns[19]. Accordingly, the observed decrease in fracture energy could be due to a change in the local mechanical properties, i.e. yield stress or elastic modulus, of the blend in the vicinity of the crack tip induced by the bonding process or by the different crystallization conditions following bonding. Although this seems to be a possible interpretation, we have no conclusive evidence for it at present.

Fracture path

The fracture path can be determined from the ESCA results in *Table 3*. For the bonds made at 225°C the compositions of both fracture surfaces are essentially the same. Small differences, less than 1%, are observed and are within the experimental error of the technique. The fracture surfaces of the PP_g/PA bond are very high in carbon and very low in nitrogen, suggesting that crack growth is through the PP_g. In a previous study, crack propagation in PP_g/PA bonds was found to occur within a thin layer of low molecular weight grafted PP adjacent to the interface[20]. Based on the ESCA data, the same conclusion is reached here, and is shown schematically in *Figure 9a*.

The composition of the fracture surfaces of the 75PP_g–25PA/PA bond also have a high carbon signal, although slightly lower than that of the PPPA fracture surfaces. The continuous phase of the 75PP_g–25PA blend is the PP_g, and crack growth occurs in a similar manner to the PP_g/PA

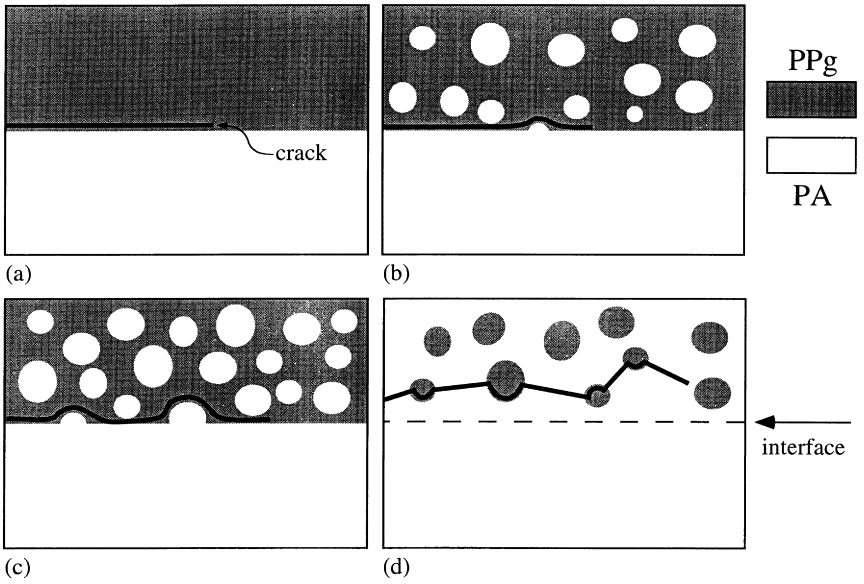

Figure 9 Path of crack propagation for: (a) PP_g–PA; (b) $75PP_g$–25PA/PA; (c) $50PP_g$–50PA/PA; and (d) $25PP_g$–75PA/PA

bonds, but is more complicated due to the presence of the PA domains. The PA domains will also be surrounded by an interlayer rich in grafted PP. Evidence of the grafted PP in this region is found in *Figure 7*, where dark areas around the PA domains indicate a higher local concentration of MAH. As the crack grows, its path is predominately near the interface, and will grow either in the region between the interface and a PA domain, or around a PA domain as shown in *Figure 9b*. The effect of the PA domains is to alter the crack propagation path which ultimately leads to the higher fracture energies observed for this blend compared with the PP_g/PA bonds.

The fracture surface composition of the $50PP_g$–50PA/PA bond made at 225°C is almost the same as those of the $75PP_g$–25PA/PA bond, but with slightly higher signals for oxygen and nitrogen. The size of the PA domains in the $50PP_g$–50PA blend is approximately the same as the $75PP_g$–25PA blend, but there are twice as many PA domains present. Their higher concentration in this blend makes crack growth more difficult and results in higher fracture energies for these bonds. The slight increase in the oxygen and nitrogen signals reflects the close proximity of the PA domains to the fracture path, as shown in *Figure 9c*.

The composition of the fracture surfaces of the $25PP_g$–75PA/PA bond is very different from the previous compositions. For this blend the continuous phase is PA, and crack propagation must occur through the PA. However, comparison with the compositions of the reference surfaces show that a significant amount of PP_g is present at the fracture surface. Thus, since the G_c of the PP_g is much lower than that of the matrix, the path of crack propagation through the $25PP_g$–75PA/PA bond will be close to the interface but pass from domain to domain of PP_g as shown in *Figure 9d*. Since the crack must grow through the tougher PA resin, the measured G_c values are nevertheless higher than that of pure PP_g. The surface of the PP_g domains will also be covered by a layer of lower molecular weight grafted PP_g and the crack will probably propagate in this layer rather than grow into the interior of the domain as shown in *Figure 9d*.

CONCLUSION

The fracture energy G_c of interfaces formed between PP_g–PA blends and pure PA depends on blends composition and bonding temperature. For bonding temperatures, T_b, below the melting temperature of PA, the fracture energy G_c of the bonds is low. G_c nevertheless increases with increasing T_b, reaching a maximum for $T_b \cong 225$°C, which approximately coincides with the melting temperature of PA, and then falling off at higher T_b. Observations of the fracture surfaces using electron spectroscopy for chemical analysis (ESCA) show that fracture occurs cohesively in the blend within a thin layer close to the interface. In the case of blends in which the PP_g is the continuous phase, the presence of the PA domains alters the crack propagation path, leading to an increase in G_c with increasing PA content. In the case of blends where the PA is the continuous phase, the fracture behaviour depends strongly on bonding temperature. For $T_b < 225$°C, PA is still solid, which prevents intimate contact and interdiffusion across the interface. G_c is low, and decreases with increasing PA content. For $T_b \geq 225$°C, melting of PA allows interdiffusion of PA chains to occur across the interface, leading to a strong bond. The experimental observations suggest that the crack propagates by jumping between PP_g domains. In this temperature range, G_c is high, and increases with increasing PA content.

ACKNOWLEDGEMENTS

The authors acknowledge Professor K. Char at Seoul National University for useful discussions and critical reading of the manuscript. We are grateful to N. Xanthopoulos and Professor H. J. Mathieu from Laboratoire de Métallurgie Chimique of Ecole Polytechnique Fédérale de Lausanne for the help in performing the ESCA measurements and B. Senior from the Centre Interdépartemental de Microscopie Electronique of Ecole Polytechnique Fédérale de Lausanne for the scanning electron microscopy. Financial support of this work was provided by the Priority Program for Materials (PPM) in Switzerland.

REFERENCES

1. Wool, R. P., *Polymer Interfaces: Structure and Strength*. Hanser/Gardner, Cincinatti, 1995.

2. Jud, K., Kausch, H.-H. and Williams, J.G., *J. Mater. Sci.*, 1981, **16**, 204.
3. Kausch, H.-H. and Tirell, M., *Ann. Rev. Mater. Sci.*, 1989, **19**, 341.
4. Kausch, H.-H., *Polymer Fracture*, 2nd edn. Springer, Heidelberg, 1987, chap. 10.
5. Smith, G. D., Toll, S. and Månson, J.-A. E., *Proceedings of 3rd International Conf. on Flow Processes in Composite Materials*, Galway, Ireland, July 7–9, 1994, p. 423.
6. Cho, K., Brown, H. R. and Miller, D. C., *J. Polym. Sci., Part B: Polym. Phys.*, 1990, **28**, 1699.
7. Brown, H.R., *Annu. Rev. Mater. Sci.*, 1991, **21**, 463.
8. Brown, H.R., *Macromolecules*, 1991, **24**, 2752.
9. Ide, F. and Hasegawa, A., *J. Appl. Polym. Sci.*, 1974, **18**, 963.
10. Nishio, T., Suzuki, Y., Kojima, K. and Kakugo, M., *J. Polym. Engng*, 1991, **19**, 123.
11. Lee, Y. and Char, K., *Macromolecules*, 1994, **27**, 2603.
12. Duvall, J., Sellitti, C., Myers, C., Hilter, A. and Baer, E., *J. Appl. Polym. Sci.*, 1994, **52**, 195.
13. Duvall, J., Sellitti, C., Myers, C., Hilter, A. and Baer, E., *J. Appl. Polym. Sci.*, 1994, **52**, 207.
14. Duvall, J., Sellitti, C., Topolkaraev, V., Hilter, A., Baer, E. and Myers, C., *Polymer*, 1994, **35**, 3948.
15. Xiao, F., Hui, C.-Y. and Kramer, E. J., *J. Mater. Sci.*, 1993, **28**, 5620.
16. Creton, C., Kramer, E. J., Hui, C.-Y. and Brown, H. R., *Macromolecules*, 1992, **25**, 3075.
17. Brown, H. R., Char, K., Deline, V. R. and Green, P. F., *Macromolecules*, 1993, **26**, 4155.
18. Char, K., Brown, H. R. and Deline, V. R., *Macromolecules*, 1993, **26**, 4164.
19. Creton, C., in *Surfaces and Interfaces in Polymers and Composites. Proc. of the European Physical Society Meeting*, Lausanne, 1997, p. 9.
20. Bidaux, J.-E., Smith, G. D., Bernet, N. and Månson, J.-A. E., *Polymer*, 1996, **37**, 1129.
21. Boucher, E., Folkers, J. P., Hervet, H., Leger, L. and Creton, C., *Macromolecules*, 1996, **29**, 774.
22. Boucher, E., Folkers, J. P., Creton, C., Hervet, H. and Leger, L., *Macromolecules*, 1997, **30**, 2102.
23. Pusset, P., Vallat, M. F., Nardin, N. and Schulz, J., *Proc. European Conf on Adhesion, EIRADH'94*, Mulhouse, 1994, p. 462.
24. Kanninen, M. F., *Int. J. Fract.*, 1973, **9**, 83.
25. Moon, H. S., Ryoo, B. K. and Park, J. K., *J. Polym. Sci., Part B: Polym. Phys.*, 1994, **32**, 1427.